



Version 4.2

## Search for the standard model Higgs boson in $\gamma\gamma$ final states at DØ

The DØ Collaboration  
URL <http://www-d0.fnal.gov>  
(Dated: July 23, 2008)

This note describes a search for a light Higgs boson in the di-photon final state using  $2.68 \pm 0.16$   $fb^{-1}$  of the DØ Run II data, collected at the Fermilab Tevatron collider from July 2002 to March 2008. Good agreement between the data and the standard model background prediction is observed. Since there is no evidence for new physics, we set 95% C.L. limits on the production cross section times the branching ratio ( $\sigma \times BR(h \rightarrow \gamma\gamma)$ ) relative to the standard model like Higgs prediction for different assumed Higgs masses. The observed limits ( $\sigma(\text{limit})/\sigma(SM)$ ) range from 21.2 to 73.4 for Higgs mass from 100 to 150 GeV, while the expected limits range from 21.7 to 40.8.

*Preliminary Results for summer 2008 Conferences*

## I. INTRODUCTION

In the standard model (SM), the  $h \rightarrow \gamma\gamma$  branching ratio is small, for instance, it is only 0.22% for a Higgs boson with a mass of 130 GeV. However, it is well-known that the SM is incomplete. In some models beyond the SM, the  $h \rightarrow \gamma\gamma$  branching ratio can be enhanced significantly, some examples can be found in Ref. [1]. The idea of the fermiophobic Higgs, which assumes zero couplings of the Higgs to the fermions, has been tested at LEP [2] - [5] and the Tevatron [6]. We examine the inclusive di-photon dataset ( $\gamma\gamma+X$ ) and search for high mass  $\gamma\gamma$  resonances. The SM Higgs is used as a possible signal model, and this analysis is a forerunner to the leading low-mass Higgs analysis at the LHC [7, 8]. There are several sizable sources of Higgs boson production within the SM. In this note, three processes: gluon gluon fusion ( $gg \rightarrow H$ ), associated production ( $VH$ ,  $V = W, Z$ ) and vector boson fusion (VBF), are taken into account, with relative cross sections as predicted by the SM. The result of the search is interpreted as upper limits on the production cross section times the branching ratio ( $h \rightarrow \gamma\gamma$ ) relative to the SM prediction for different assumed Higgs masses.

## II. DØ DETECTOR AND DATA SAMPLE

The DØ detector is comprised of a central tracking system in a 2 T superconducting solenoidal magnet, a liquid-argon/uranium calorimeter, a central preshower detector and a muon spectrometer [9]. The major parts of the DØ detector used in event selection are the tracking system, electromagnetic (EM) calorimeter and central preshower detector (CPS). The tracking system consists of a silicon microstrip tracker (SMT) and an eight-layer scintillating fiber tracker (CFT) mounted on thin coaxial barrels. It provides coverage for charged particles in the pseudorapidity range  $|\eta| < 3$  (where the pseudorapidity is defined as  $\eta \equiv -\ln[\tan(\frac{\theta}{2})]$ , with  $\theta$  denoting the polar angle with respect to the proton beam direction.) The calorimeter has a central section (CC) covering up to  $|\eta| \approx 1.1$ , and two end components (EC) extending coverage to  $|\eta| \approx 4.2$ . Each is housed in a separate cryostat. Each section is divided into EM layers on the inside and hadronic layers on the outside. The EM calorimeter has four longitudinal layers and transverse segmentation of  $0.1 \times 0.1$  in  $\eta - \phi$  space (where  $\phi$  is the azimuthal angle), except in the third layer, where it is  $0.05 \times 0.05$ . Immediately before the inner layer of the central EM calorimeter, there is a central preshower detector (CPS) formed of  $2X_0$  of absorber followed by several layers of scintillating strips with embedded wavelength-shifting fibers. Luminosity is measured using plastic scintillator arrays located in front of the EC cryostats, covering  $2.7 < |\eta| < 4.4$ . The data acquisition system consists of a three-level trigger, designed to accommodate the high instantaneous luminosity. For final states containing two photon candidates with transverse momentum ( $p_T$ ) above 25 GeV, the trigger efficiency is close to 100%. The data samples used in this analysis were collected between July 2002 and March 2008 and corresponds to an integrated luminosity of  $2.68 \pm 0.16 \text{ fb}^{-1}$ .

## III. EVENT SELECTION

For each event, at least two photon candidates in the central calorimeter region are selected, and the leading and sub-leading  $p_T$  photon candidates must : (i) have  $p_T > 25.0$  GeV; (ii) deposit at least 97% of the cluster energy in the EM section of the calorimeter; (iii) have the calorimeter isolation variable ( $I$ ) less than 0.1, where  $I \equiv \frac{E_{\text{tot}}(0.4) - E_{\text{EM}}(0.2)}{E_{\text{EM}}(0.2)}$ ,  $E_{\text{tot}}(0.4)$  is the total shower energy in a cone of radius 0.4, and  $E_{\text{EM}}(0.2)$  the EM energy in a cone of radius 0.2 around the photon candidate direction; (iv) have no track pointing to them and hits density in SMT and CFT are not consistent with that of a track associated with an electron; (v) have the artificial neural network (ANN) output variable  $O_{NN} > 0.05$  (0.1) for the two different data taking periods to reduce most of the jet background, where the  $O_{NN}$  is an ANN discriminant variable that combines five characteristic variables using the EM calorimeter and CPS information:

- number of EM1 cells in a cone of radius 0.2,
- number of EM1 cells in a hollow cone  $0.2 < \Delta R < 0.4$ ,
- scalar sum of transverse momenta of the excluded tracks in annulus cone  $0.05 < \Delta R < 0.4$ ,
- number of CPS clusters in a cone of radius 0.1,
- energy-squared-weighted RMS of CPS.

The ANN is built using JETNET package [12], and is trained with di-photon and di-jet MC samples generated using PYTHIA [10] and fully simulated using the GEANT-3 based Dzero detector simulations [11]. It is tested on the  $Z+\gamma$  data with  $Z$  boson decaying to  $\mu^+\mu^-$  and  $e^+e^-$ . The  $O_{NN}$  distributions for the photon candidates from  $Z+\gamma$  data, the QCD di-photon MC samples and the fake photon candidates in jet MC samples are shown in Fig. 1.

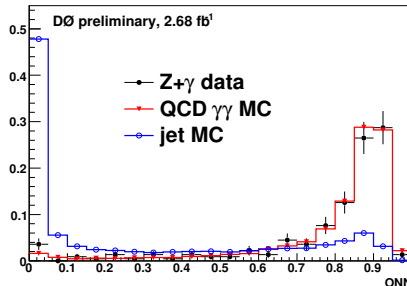


FIG. 1: Normalized distributions of  $O_{NN}$  value from real and fake photons.

#### IV. BACKGROUNDS

There are three major sources of background to the  $h \rightarrow \gamma\gamma$  signature: (i) Drell-Yan events, where both electrons are misidentified as photons; (ii)  $\gamma$ +jet and di-jet events where the jet(s) are mis-identified as photon(s); (iii) direct QCD di-photon events.

##### A. Drell-Yan $Z/\gamma^* \rightarrow ee$ contribution

We use  $Z/\gamma^* \rightarrow ee$  PYTHIA [10] Monte Carlo samples to estimate the Drell-Yan contribution. The next-to-next-to-leading-order (NNLO)  $p\bar{p} \rightarrow Z/\gamma^* \rightarrow ee$  cross section of  $254 \pm 10$  pb [13] for 60 - 130 GeV region is used for the absolute normalization. From the  $Z/\gamma^* \rightarrow ee$  MC samples, we find that 2.0% of the electrons can satisfy the photon selection requirements described in Section III due to the tracking inefficiencies. The total background contribution from Drell-Yan process is found to be  $92.8 \pm 11.3$ .

##### B. $\gamma$ +jet and di-jet background

We estimate the  $\gamma$  + jet and di-jet contributions to the data with the final event selection applied (see section III) by using a  $4 \times 4$  matrix background subtraction method. The method is described in Ref. [15]. In this analysis, we use  $O_{NN} = 0.75$  as a boundary to classify the candidates into four categories:

- $N_{pp}$  of them have both photon candidates with  $O_{NN} > 0.75$ ;
- $N_{pf}$  of them have the leading photon candidate with  $O_{NN} > 0.75$ , but the sub-leading  $O_{NN} < 0.75$ ;
- $N_{fp}$  of them have the leading photon candidate with  $O_{NN} < 0.75$ , but the sub-leading  $O_{NN} > 0.75$ ;
- $N_{ff}$  of them have both photon candidates with  $O_{NN} < 0.75$ ;

The Drell-Yan  $Z/\gamma^* \rightarrow ee$  contributions to  $(N_{pp}, N_{pf}, N_{fp}, N_{ff})$  are determined from MC simulations and are removed. The pass-fail vector  $(N_{pp}, N_{pf}, N_{fp}, N_{ff})$  thus obtained is related the  $(N_{\gamma\gamma}, N_{\gamma j}, N_{j\gamma}, N_{jj})$  vector as follows:

$$\begin{pmatrix} N_{ff} \\ N_{fp} \\ N_{pf} \\ N_{pp} \end{pmatrix} = E \times \begin{pmatrix} N_{jj} \\ N_{j\gamma} \\ N_{\gamma j} \\ N_{\gamma\gamma} \end{pmatrix} \quad (1)$$

where the  $N_{\gamma\gamma}$  is the number of  $\gamma+\gamma$  events,  $N_{\gamma j}$  and  $N_{j\gamma}$  are the number of  $\gamma$ +jet events and  $N_{jj}$  is the number of di-jet events. The  $4 \times 4$  matrix  $E$  is defined as:

$$\begin{pmatrix} (1-\epsilon_{j1})(1-\epsilon_{j2}) & (1-\epsilon_{j1})(1-\epsilon_{\gamma2}) & (1-\epsilon_{\gamma1})(1-\epsilon_{j2}) & (1-\epsilon_{\gamma1})(1-\epsilon_{\gamma2}) \\ (1-\epsilon_{j1})\epsilon_{j2} & (1-\epsilon_{j1})\epsilon_{\gamma2} & (1-\epsilon_{\gamma1})\epsilon_{j2} & (1-\epsilon_{\gamma1})\epsilon_{\gamma2} \\ \epsilon_{j1}(1-\epsilon_{j2}) & \epsilon_{j1}(1-\epsilon_{\gamma2}) & \epsilon_{\gamma1}(1-\epsilon_{j2}) & \epsilon_{\gamma1}(1-\epsilon_{\gamma2}) \\ \epsilon_{j1}\epsilon_{j2} & \epsilon_{j1}\epsilon_{\gamma2} & \epsilon_{\gamma1}\epsilon_{j2} & \epsilon_{\gamma1}\epsilon_{\gamma2} \end{pmatrix} \quad (2)$$

where  $\epsilon_{\gamma1}$  and  $\epsilon_{\gamma2}$  are the fractions of the leading and sub-leading photons that have passed the event selection and have  $O_{NN} > 0.75$ , and  $\epsilon_{j1}$  and  $\epsilon_{j2}$  are the fractions of jets that have passed the event selection and have  $O_{NN} > 0.75$ . ( $N_{\gamma\gamma}, N_{\gamma j}, N_{j\gamma}, N_{jj}$ ) can be obtained by solving the linear equation. Table I shows the results after applying the method on the real data.

Total events	5068.4
$N_{\gamma\gamma}$	$2944.4 \pm 136.8$
$N_{\gamma j} + N_{j\gamma}$	$1559.6 \pm 141.9$
$N_{jj}$	$564.4 \pm 88.1$
non- $\gamma\gamma$	$2124.0 \pm 167.4$

TABLE I: The number of  $\gamma\gamma$ ,  $\gamma$ +jet, di-jet and non- $\gamma\gamma$  ( sum of  $\gamma$ +jet and di-jet ) events in the data samples from the 4x4 matrix method. The quoted uncertainties include statistical uncertainties only.

We reverse the event selection  $O_{NN}$  cut (0.05/0.1) on one of the two photon candidates to get an enriched non- $\gamma\gamma$ ( $\gamma$ +jet,di-jet) sample from data. Fig. 2 shows that the shape of the di-photon mass distribution from such ‘‘reversed-ONN’’ sample is in good agreement with the results from the  $4 \times 4$  matrix method. Given the good agreement between

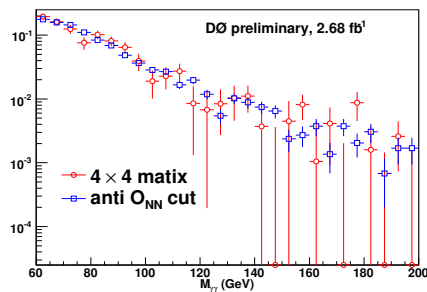


FIG. 2: non- $\gamma\gamma$  component invariant mass distribution from  $4 \times 4$  matrix background subtraction and from reversing  $O_{NN}$  cut. The area of both histograms are normalized to unity.

the distribution from the two orthogonal samples and the low statistics of the results from the matrix method, we use the ‘‘reversed-ONN’’ sample to determine the shape of the non- $\gamma\gamma$  background. In order to smooth out statistical fluctuations, we fit the mass distribution with an exponential function  $f(M_{non}) = \exp(p_0 \cdot M_{non}^2 + p_1 \cdot M_{non} + p_2)$  with  $M_{non}$  denoting the mass of the two photon candidates. The estimation of the total number of non- $\gamma\gamma$  events from the  $4 \times 4$  matrix method is used to fix the normalization. The systematic uncertainty from the shape function is taken into account when calculating the limits.

### C. Direct QCD di-photon production

We obtain a di-photon invariant mass distribution (with Drell-Yan, non- $\gamma\gamma$  subtracted off) and use the side-band fitting method to determine the QCD di-photon under the Higgs peaks. For each assumed Higgs mass ( $M_{\text{Higgs}}$ ), we use the simple exponential function  $f(M_{diem}) = \exp(p_0 \cdot M_{diem}^2 + p_1 \cdot M_{diem} + p_2)$  to fit the di-photon mass distribution in the [70, 200] GeV range outside of the signal mass region ( $M_{\text{Higgs}}-15$  GeV,  $M_{\text{Higgs}}+15$  GeV). We then interpolate the function to the signal region to determine the QCD di-photon contribution.

## V. SYSTEMATIC UNCERTAINTIES

The uncertainty of the  $O_{NN} > 0.75$  efficiencies for the photon and photon-like jets is the source of the uncertainty of the background subtraction. We adopt the difference in the number of background events from the mean efficiencies and the upper and lower uncertainty bands as the systematic uncertainty. The influence of the parton distribution functions (PDF) uncertainty on the acceptance is 1.7% - 2.2% depending on the Higgs mass, estimated from CTEQ6M [18] error functions, where we use the cross section to do the weight between three different signal processes. Table II lists all the systematic uncertainties of this analysis:

source	uncertainty
luminosity	6.1% [17]
trigger	0.1%
PDF for $h \rightarrow \gamma\gamma$ acceptance	1.7% - 2.2%
ID efficiency	1.0%
Track Isolation efficiency	0.4%
photon "no-track" and HOR efficiency	2.2%
$Z/\gamma^*(ee)$ cross section	3.9%
electron track match inefficiency	6.8%
background subtraction	0.6% - 3.8%

TABLE II: Systematic uncertainties.

## VI. FINAL EVENT DISTRIBUTIONS AND LIMITS

### A. Final event distributions

Figure 3 shows the final invariant mass of the two-photon candidates in the interval of ( $M_{Higgs}-15$  GeV,  $M_{Higgs}+15$  GeV) for each assumed Higgs mass. The shaded region correspond to the expected background error band. The inner band represents the statistical uncertainty, while the outer represents the systematic uncertainty. Table III and Table IV show the number of events in data, expected background and signal in each mass interval for different SM Higgs mass values.

$M_{Higgs}$	100 GeV	110 GeV	120 GeV	130 GeV	140 GeV	150 GeV
$\epsilon_{sel}(ggH)$	0.185±0.001	0.191±0.001	0.196±0.001	0.201±0.001	0.204±0.001	0.207±0.001
$\epsilon_{sel}(VH)$	0.178±0.001	0.191±0.001	0.197±0.001	0.204±0.001	0.213±0.001	0.214±0.001
$\epsilon_{sel}(VBF)$	0.196±0.001	0.208±0.001	0.215±0.002	0.223±0.001	0.227±0.002	0.233±0.002
$Z/\gamma^* \rightarrow ee$	56.5±7.5	22.1±3.7	6.4±1.7	2.1±0.9	1.5±0.8	0.8±0.5
QCD $\gamma\gamma$	699.1±37.0	420.1±31.4	290.0±22.8	209.3±14.4	146.1±8.9	112.0±6.6
$\gamma j+jj$	463.1±14.5	283.7±8.8	179.0±5.5	116.4±3.6	78.0±2.4	53.8±1.6
total background	1218.7±41.3	725.9±38.2	476.0±29.6	327.5±16.2	225.6±9.8	166.6±6.9
data	1272	768	513	333	255	188
signal	1.42±0.09	1.41±0.09	1.31±0.09	1.10±0.07	0.78±0.05	0.46±0.03

TABLE III: Event selection efficiencies( $\epsilon_{sel}$ ) with their statistical error and number of events in data and the background estimation in the mass interval of ( $M_{Higgs}-15$  GeV,  $M_{Higgs} + 15$  GeV) with  $M_{Higgs}$  varying from 100 GeV to 150 GeV.

### B. Limit setting

Since there is no excess observed above the background expectation, we proceed to set upper limits on the Higgs production cross section times branching ratio for Higgs decaying into a pair of photons. The distributions of invariant mass of the two photon candidates in the interval of ( $M_{Higgs}-15$  GeV,  $M_{Higgs} + 15$  GeV) (shown in Fig. 3) are used for this purpose. Limits are calculated at the 95% confidence level using the modified frequentist CLs approach with a Poisson log-likelihood ratio test statistic [19, 20]. The impact of systematic uncertainties is incorporated through marginalization of the Poisson probability distributions for signal and background via Gaussian distribution. All

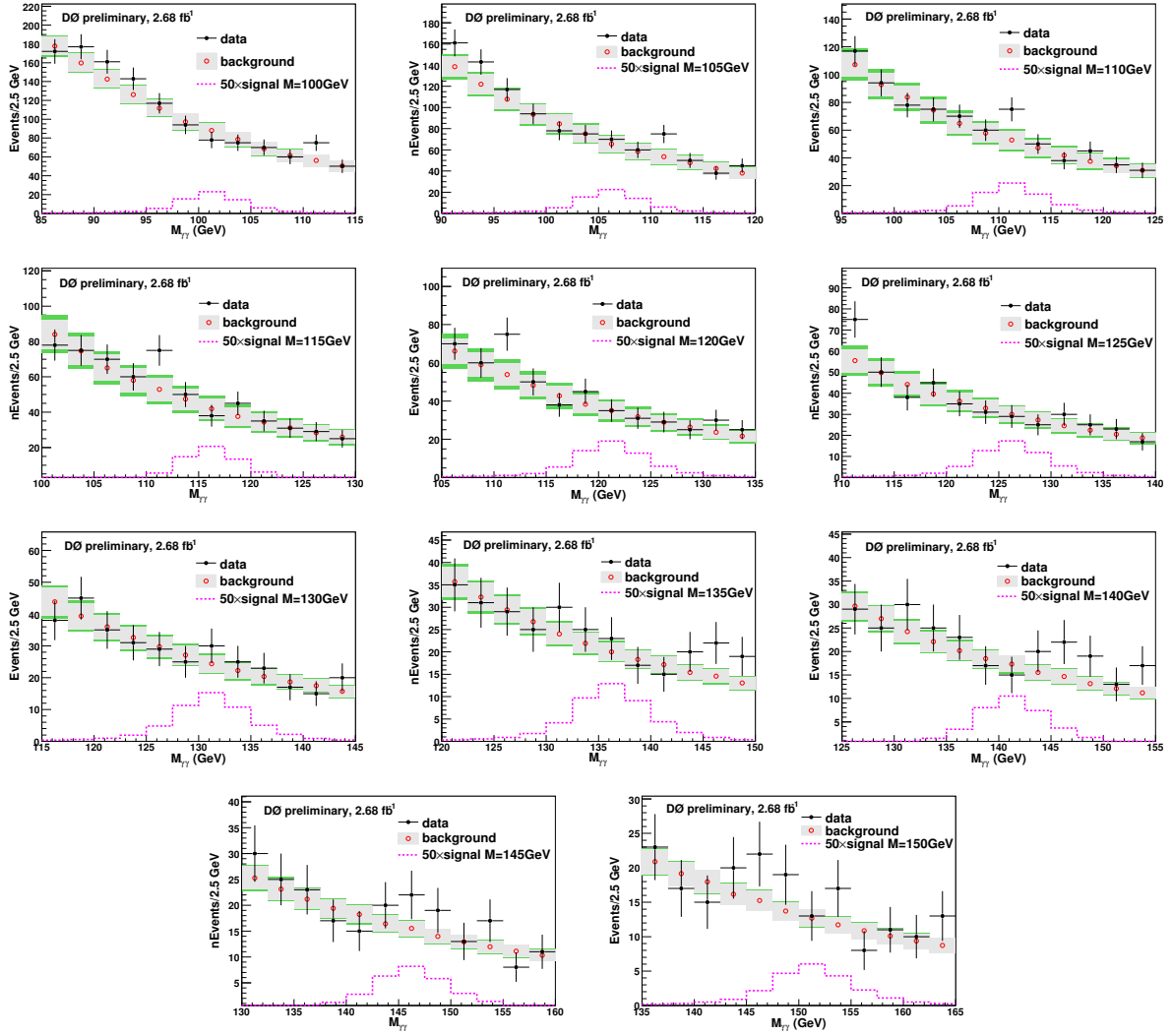


FIG. 3: Invariant mass distribution of the two photon candidates in the mass interval of  $(M_{Higgs}-15 \text{ GeV}, M_{Higgs}+15 \text{ GeV})$  for different Higgs masses.

correlations in systematic uncertainties are maintained between signal and background. The expected distributions for background are evaluated by minimizing a profile likelihood function, referencing the shape and rate of the observed distributions in the full distribution [20]. Table V shows the limits on  $\sigma \times BR$  for the different Higgs masses. Table VI shows the limits on  $\sigma \times BR$  relative to the SM prediction for different Higgs masses. The corresponding plot is Fig. 4. The SM  $\sigma \times BR$  values are extracted from Ref. [21].

$M_{\text{Higgs}}$	105 GeV	115 GeV	125 GeV	135 GeV	145 GeV
$\epsilon_{sel}(\text{ggH})$	$0.188 \pm 0.001$	$0.194 \pm 0.001$	$0.199 \pm 0.001$	$0.203 \pm 0.001$	$0.206 \pm 0.001$
$\epsilon_{sel}(\text{VH})$	$0.180 \pm 0.001$	$0.194 \pm 0.001$	$0.201 \pm 0.001$	$0.209 \pm 0.002$	$0.230 \pm 0.002$
$\epsilon_{sel}(\text{VBF})$	$0.202 \pm 0.001$	$0.212 \pm 0.002$	$0.219 \pm 0.002$	$0.225 \pm 0.002$	$0.229 \pm 0.002$
$Z/\gamma^* \rightarrow ee$	$38.5 \pm 5.5$	$13.5 \pm 2.7$	$4.5 \pm 1.4$	$2.2 \pm 0.9$	$0.8 \pm 0.5$
QCD $\gamma\gamma$	$528.3 \pm 25.5$	$343.3 \pm 20.4$	$253.5 \pm 13.1$	$171.6 \pm 7.7$	$134.1 \pm 5.4$
$\gamma j + jj$	$361.1 \pm 8.0$	$224.5 \pm 4.9$	$143.8 \pm 3.1$	$94.9 \pm 2.0$	$64.5 \pm 1.4$
total background	$927.9 \pm 31.2$	$581.3 \pm 27.9$	$401.8 \pm 17.8$	$268.6 \pm 9.2$	$199.4 \pm 6.3$
data	1006	611	423	291	220
signal	$1.42 \pm 0.09$	$1.34 \pm 0.09$	$1.21 \pm 0.08$	$0.94 \pm 0.06$	$0.62 \pm 0.04$

TABLE IV: Event selection efficiencies( $\epsilon_{sel}$ ) with their statistical error and number of events in data and the background estimation in the mass interval of ( $M_{\text{Higgs}}-15$  GeV,  $M_{\text{Higgs}} + 15$  GeV) with  $M_{\text{Higgs}}$  varying from 105 GeV to 145 GeV.

Higgs mass (GeV)	100	105	110	115	120	125	130	135	140	145	150
observed limits (fb)	67.9	101.1	150.7	86.5	64.1	51.2	66.3	60.9	58.0	73.8	64.1
expected limits (fb)	92.4	85.5	74.2	65.1	62.8	52.4	49.0	43.8	41.8	38.3	35.6

TABLE V: 95% C.L. limits on  $\sigma \times BR$  for the different Higgs masses.

Higgs mass (GeV)	100	105	110	115	120	125	130	135	140	145	150
observed limits	22.2	33.6	51.4	30.8	24.3	21.2	31.0	33.4	38.7	62.8	73.4
expected limits	30.2	28.4	25.3	23.2	23.8	21.7	22.9	24.0	27.9	32.6	40.8

TABLE VI: 95% C.L. limits on  $\sigma \times BR$  relative to the SM prediction for different Higgs masses.

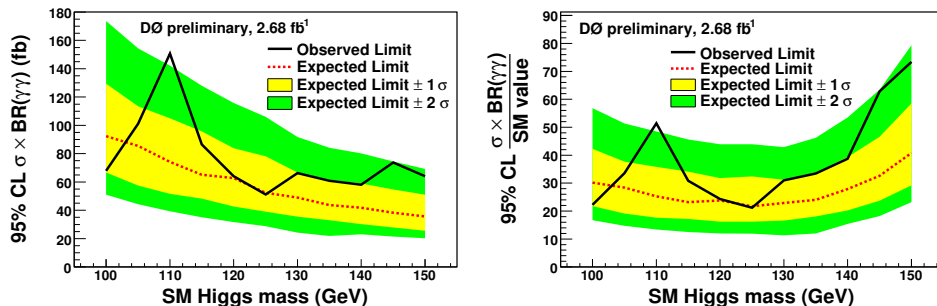


FIG. 4: Left plot shows the limits on the  $\sigma \times BR$  for the different Higgs masses, right plot shows the 95% C.L. limits on the  $\sigma \times BR$  relative to the SM prediction for different Higgs masses.

## VII. SUMMARY

This note describes a search for the SM Higgs boson in the di-photon channel in 2.68 fb<sup>-1</sup> DØRun II data. The data and SM background estimation are consistent, so we set the 95% C.L. limits on the  $\sigma \times BR$  relative to the SM prediction for different SM Higgs masses. The observed limits ( $\sigma(\text{limit})/\sigma(\text{SM})$ ) are from 21.2 to 73.4 for Higgs mass from 100 to 150 GeV, while the expected limits range from 21.7 to 40.8.

## Acknowledgments

We thank the staffs at Fermilab and collaborating institutions, and acknowledge support from the DOE and NSF (USA); CEA and CNRS/IN2P3 (France); FASI, Rosatom and RFBR (Russia); CAPES, CNPq, FAPERJ, FAPESP and FUNDUNESP (Brazil); DAE and DST (India); Colciencias (Colombia); CONACyT (Mexico); KRF and KOSEF (Korea); CONICET and UBACyT (Argentina); FOM (The Netherlands); STFC (United Kingdom); MSMT and GACR (Czech Republic); CRC Program, CFI, NSERC and WestGrid Project (Canada); BMBF and DFG (Germany); SFI (Ireland); The Swedish Research Council (Sweden); CAS and CNSF (China); and the Alexander von Humboldt Foundation.

- 
- [1] S. Mrenna and J. Wells, arXiv:hep-ph/0001226, (2000).
  - [2] A. Heister et al. (ALEPH Collaboration), Phys. Lett. B **544**, 16 (2002).
  - [3] P. Abreu et al. (DELPHI Collaboration), Phys. Lett. B **507**, 89 (2001); Eur. Phys. J. C **35**, 313, (2004).
  - [4] G. Abbiendi et al. (OPAL Collaboration), Phys. Lett. B **544**, 44 (2002).
  - [5] P. Achard et al. (L3 Collaboration), Phys. Lett. B **534**, 28 (2002); Phys. Lett. B **568**, 191 (2003).
  - [6] DØ Collaboration, "Search for Light Higgs Boson in  $\gamma\gamma+X$  Final State with the DØ Detector at  $\sqrt{s} = 1.96$  TeV", DØ Note **5426-CONF** (2007).
  - [7] ATLAS Calorimeter Performance, TDR-1, CERN/LHCC 96-40, December 1996.
  - [8] CMS ECAL Technical Design Report, CERN/LHCC 97-33, CMS TDR 4, 15 December 1997.
  - [9] V. M. Abazov *et al.*, Nucl. Instrum. Meth. A **565**, 463 (2006).
  - [10] T.Sjöstrand *et al.*, hep-ph/0108264,LU-TP-01-21,Lund2001
  - [11] R. Brun and F. Carminati, CERN Program Library Long Writeup, Report No. W5013, 1993.
  - [12] C. Peterson, T. Rognvaldsson and L. Lonnblad, "JETNET 3.0 A versatile Artificial Neural Network Package", Lund University Preprint LU-TP 93-29. Version 3.5 is used here.
  - [13] R. Hamberg, W. L. van Neerven and T. Matsuura, Nucl. Phys. B **359**, 343 (1991) [Erratum-ibid. B **644**, 403 (2002)].
  - [14] T. Binoth, J. Ph.Guillet, E. Pilon, and M. Werlen, Eur. Phys. J. C. **16**, 311 (2000).
  - [15] Y. Liu, Ph.D. thesis, Fermilab [FERMILAB-THESIS-2004-37] (2004).
  - [16] D. Acosta *et al.* (CDF collaboration), Phys. Rev. Lett. **95**, 022003 (2005).
  - [17] T. Andeen *et al.*, FERMILAB-TM-2365 (2007).
  - [18] J. Pumplin *et al.*, JHEP **0207**, 012 (2002).
  - [19] W. Fisher, FERMILAB-TM-2386-E (2006).
  - [20] T. Junk, Nucl. Instrum. Meth. A **434**, 435 (1999); A. Read, CERN 2000-005 (30 May 2000).
  - [21] <http://maltoni.web.cern.ch/maltoni/TeV4LHC/SM.html> .